

The general aspects of noise in analogue hardware deep neural networks

N. Semenova,^{1,2,a)} L. Larger,¹ and D. Brunner¹

¹⁾*Département d'Optique P. M. Duffieux, Institut FEMTO-ST, Université Bourgogne-Franche-Comté CNRS UMR 6174, Besançon, France.*

²⁾*Department of Physics, Saratov State University, 83 Astrakhanskaya str., 410012 Saratov, Russia.*

(Dated: 1 March 2025)

Deep neural networks unlocked a vast range of new applications by solving tasks of which many were previously deemed as reserved to higher human intelligence. One of the developments enabling this success was a boost in computing power provided by special purpose hardware, such as graphic or tensor processing units. However, these do not leverage fundamental features of neural networks like parallelism and analog state variables. Instead, they emulate neural networks relying on computing power, which results in unsustainable energy consumption and comparatively low speed. Fully parallel and analogue hardware promises to overcome these challenges, yet the impact of analogue neuron noise and its propagation, i.e. accumulation, threatens rendering such approaches inept. Here, we analyse for the first time the propagation of noise in parallel deep neural networks comprising noisy nonlinear neurons. We develop an analytical treatment for both, symmetric networks to highlight the underlying mechanisms, and networks trained with back propagation. We find that noise accumulation is generally bound, and adding additional network layers does not worsen the signal to noise ratio beyond this limit. Most importantly, noise accumulation can be suppressed entirely when neuron activation functions have a slope smaller than unity. We therefore developed the framework for noise of deep neural networks implemented in analog systems, and identify criteria allowing engineers to design noise-resilient novel neural network hardware.

A fundamental aspect of neural networks (NNs) is the propagation of information between nodes along weighted connections, making parallelism an essential prerequisite for an efficient implementation. However, current digital computing architectures are mostly serial and spatially separate memory from information transformation. Maximal computing performance can only be achieved if a NN's topology is faithfully reproduced by the hardware substrate. In such systems, the overhead due to serial communication is avoided: each neuron corresponds to a simple nonlinear component, each connection to a direct physical link.

Motivated by the potential benefits, research activity along these lines¹ has lately exploded. Novel physical components such as lasers², memristors³ and spin-torque oscillators⁴ have been shown to serve as excellent analogue neurons. Simultaneously, mostly optical concepts for parallel networks based on holography⁵, diffraction^{6,7}, meshes of integrated Mach-Zehnder interferometers⁸, wavelength division multiplexing⁹ and 3D printed optical interconnects¹⁰⁻¹² have demonstrated fully parallel networking.

Yet, the physical realization of NNs in mostly analogue substrates fundamentally modifies the context in which information is maintained during computation. Ignoring digitization noise¹³, digital computers are essentially noise-less, and at least in principle signals are perfectly maintained during transduction and transformation. NNs comprising analogue neurons and physical connections, however, exhibit noise typically from var-

ious sources with different properties. In optical NNs noise can be induced by lasers, electro-optical modulators and other components^{14,15} are generally prone to noise. Hardware weights can for example be implemented using phase change materials¹⁶, which potentially exhibit thermal and parametric noise induced by internal as well as external perturbations. Analog electronic processors based on binary neural networks showed the impact of comparator noise on accuracy¹⁷. Analog electronic multi-layer perceptrons are sensitive on temperature and voltage fluctuations as source of noise¹⁸. The central importance of noise for future NN hardware solutions is therefore moving into focus, work remains restricted on particular hardware¹⁹⁻²² rather than on the general principles of noise in NNs. The origin of noise must generally be considered diverse and will differ depending on the NN hardware substrate. Most relevant noise sources can be differentiated into four main classes: additive and multiplicative, correlated and uncorrelated noise.

In our previous work we considered the impact of noise on feed-forward and recurrent NNs comprising only linear neurons and networks with uniform, i.e. untrained connections¹⁵. This enabled the observation and description exclusively focusing on the beneficial or detrimental role of NN connections upon the propagation of the different noise types. Here, we numerically and analytically investigate the general aspects of noise in deep neural networks (DNNs) comprising nonlinear neurons. Importantly, we trained our DNNs according to standard error back-propagation and develop an analytical concept that incorporates the effect of training only relying on statistical connectivity measures. We demonstrate excellent accuracy of our mathematical framework for DNNs trained in classification and analogue function approxi-

^{a)}Electronic mail: nadya.i.semenova@gmail.com

mation, hence for the vast majority of tasks in the machine learning context.

We find that nonlinear neurons decorrelate noise otherwise correlated across neuron populations. Previously we identified such correlated noise as the most relevant perturbation, and noteworthy nonlinearity can therefore be beneficial for a NNs signal to noise ratio (SNR). Our most important finding however is that noise propagation between consecutive network layers can be stopped completely, i.e. the accumulation of noise can be avoided. We derive the general conditions for such noise-freezing and show that these are easily met in DNN concepts as well as hardware. Finally, even without such noise freezing, a DNN's SNR is generally bound and increasing its depth does not further reduce its SNR below a limit.

I. NEURAL NETWORKS AND NOISY NEURONS

A. Deep neural networks

DNNs may be found in multiple configurations, which can be categorized according to their connection topology. A simple DNN comprising input and output layers, each comprising a single linear neuron, plus two hidden layers hosting the nonlinear neurons is schematically illustrated in Fig. 1. Each neuron is identified by its layer index $n \in [1; N]$ and intralayer position $i \in [1; I_n]$ with N and I_n as the number of layers and neurons in a particular layer, respectively. At each integer instant $t \in [1; T]$ the network receives input signal \mathbf{u}^t .

In general, a neuron's internal state $\tilde{x}_{n,i}^t$ combines input from other neurons according to connectivity weight matrix \mathbf{W}

$$\tilde{x}_{n,i}^t = \sum_{j=1}^{I_{n-1}} W_{i,j}^n y_{n-1,j}^t + b_{n,i}, \quad (1)$$

where $b_{n,i}$ is a constant bias and $y_{n-1,j}^t$ is the output signal of the j th neuron in the $(n-1)$ th layer. Equation (1) is valid for hidden and output layers, while for the input layer $\tilde{x}_{1,i}^t = u_i^t$. Internal states are typically transformed by a nonlinear function $f(\cdot)$, creating the neuron's output

$$x_{n,i}^t = f(\tilde{x}_{n,i}^t). \quad (2)$$

Here, we consider sigmoid $f(\tilde{x}) = \frac{1}{2} + \frac{\alpha(\tilde{x}-0.5)}{2\sqrt{1+\alpha^2(\tilde{x}-0.5)^2}}$ as the neurons' nonlinearity. We shifted the sigmoid to have its inflection point at $\tilde{x} = 0.5$, and parameter α determines the slope.

A basic aspect of mapping with a nonlinear function $f(\cdot)$ is that a uniformly distributed input results in a non-uniformly distributed output. Nonlinear functions typically have sections with a low gradient, and for example the here used shifted sigmoid exhibits two horizontal asymptotes at $f(\tilde{x}) = 0$ and $f(\tilde{x}) = 1$. It is in the vicinity of these asymptotes where the output signal is mainly

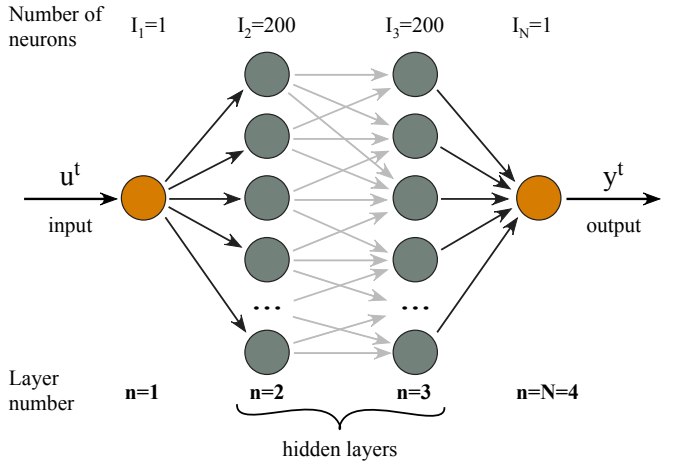


FIG. 1. Schematic illustration of a deep neural network.

concentrated, i.e. focused, and we refer to these zones as *focusing points*. For the rest of this manuscript we use a network with $N = 4$, $I_1 = I_4 = 1$ and $I_2 = I_3 = 200$ as well as an input signal for length $T = 1000$.

B. Relevant types of noise

In experiments with analogue hardware NNs we carefully characterized noise present in the system^{15,23}. In order to draw general conclusions we will consider additive and multiplicative noise, which were shown to be most relevant. Furthermore, both are perturbations commonly found in hardware.

Additive noise is added to noiseless signal x_i according to $y_i = x_i + \sqrt{2D_A}\xi^A$, while multiplicative noise has a multiplicative relationship $y_i = x_i \cdot (1 + \sqrt{2D_M}\xi^M)$. Here, D_A and D_M are the intensity for additive and multiplicative noise, respectively, while $\xi^{A|M}$ are the corresponding noise sources drawn from a normalized random Gaussian distribution. Moreover, noise inside a group of neurons can be correlated or uncorrelated. In the latter case, noise affects each neuron differently at each instant t , while correlated noise identically perturbs the neurons within such a group at each t . Combined, correlated additive $\xi^{C,A}$ and multiplicative $\xi^{C,M}$, uncorrelated additive $\xi^{U,A}$ and multiplicative $\xi^{U,M}$ noise perturb a signal according to

$$y_{n,i}^t = \sqrt{2D_A^U}\xi_{n,i}^{U,A} + \sqrt{2D_M^C}\xi_n^{C,A} + x_{n,i}^t \cdot (1 + \sqrt{2D_M^U}\xi_{n,i}^{U,M}) (1 + \sqrt{2D_M^C}\xi_n^{C,M}). \quad (3)$$

The canonical mechanisms of each of these is shown in Fig. 2. Here, we consider that noise is correlated for neurons contained within the same layer.

The main property of interest is the SNR encountered at a DNN's output. The SNR is obtained by dividing a signal's mean value by the square root of its variance. We numerically determine the variance by repeating the

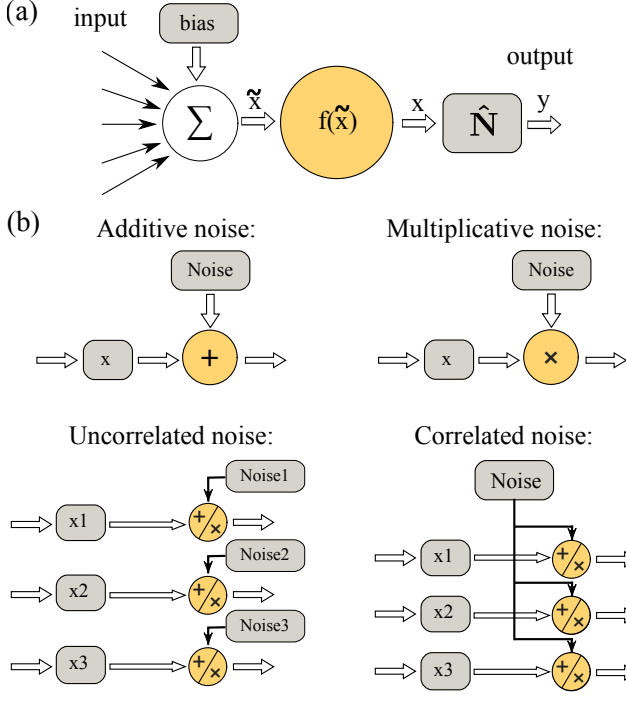


FIG. 2. (a) Schematic of a nonlinear neuron with noise. The nonlinear output $x = f(\tilde{x})$ is perturbed by noise operator \hat{N} with additive and multiplicative noise. (b) Schematic illustration of different types of noise sources and their action upon a signal. From¹⁵.

same input $k \in [1; K]$ times and hence this index is added to the neurons' noisy states $x_{n,i}^{t,k}$. Here, we use $K = 300$. The SNR for the i th neuron from the n th layer is

$$\text{SNR}(y_{n,i}^t) = \frac{\text{E}(y_{n,i}^t)}{(\text{Var}(y_{n,i}^t))^{1/2}}, \quad (4)$$

where $\text{E}(\cdot)$ and $\text{Var}(\cdot)$ are a variable's expectation value and variance, respectively. For simplicity we define the SNR based on variance rather than standard deviation, which is the square root of variance, as this simplifies the following derivations and equations.

For a single neuron with Gaussian distributed and zero mean additive and multiplicative, correlated and uncorrelated noise (as in Eq. (1)), the expectation value and variance are

$$\begin{aligned} \text{E}(y_{n,i}^t) &= \text{E}(x_{n,i}^t), \\ \text{Var}(y_{n,i}^t) &= \sigma_+^2 + \sigma_x^2 (\text{E}(y_{n,i}^t))^2 + (1 + \sigma_x^2) \hat{\mathbf{F}}(\tilde{x}_{n,i}^t), \end{aligned} \quad (5)$$

where $\sigma_+^2 = 2D_A^C + 2D_A^U$, $\sigma_x^2 = 2D_M^C + 2D_M^U + 4D_M^C D_M^U$ are the overall impact of additive and multiplicative noise, respectively. Operator $\hat{\mathbf{F}}$ corresponds to the variance of a random variable under the action of a nonlinear function $f(\cdot)$, in which case $\text{Var}(x_{n,i}^t) = \hat{\mathbf{F}}(\tilde{x}_{n,i}^t)$, while for a linear neuron $\text{Var}(x_{n,i}^t) = \alpha^2 \text{Var}(\tilde{x}_{n,i}^t)$.

In the case of one isolated nonlinear neuron, see gray dashed data in Fig. 3, additive noise results in an SNR

that increases linearly with the signal amplitude, and its slope is determined by noise intensity D_A . Purely multiplicative noise results in a constant level SNR for any output value. Mixed noise is characterised by a linear increase for small signal values, which for large signal amplitudes approaches the constant SNR-limit induced by multiplicative noise. The shape and law determining the SNR of individual neurons are therefore identical for linear and nonlinear neurons. Nonlinearity's only impact are the focusing points, and thus nonlinearity changes only the distribution of points along a single neuron's SNR curve. More details about individual noisy neurons in linear DNNs can be found in¹⁵, where we studied noise in feedforward and recurrent neural network with predefined, hence untrained coupling topologies. This simplification was made to separate the impact of noise and nonlinear function and we demonstrated that noise affects the final output signal differently depending on the type of noise.

Variance $\text{Var}(\tilde{x}_{n,i}^t)$ is the average noise impact from the previous layer $n-1$ and comprises contributions from correlated noise N_n^C , uncorrelated noise N_n^U and noise N_n^{prev} from the layer preceding the previous one

$$\begin{aligned} \text{Var}(\tilde{x}_{n,i}^t) &= N_n^C + N_n^U + N_n^{\text{prev}} \\ N_n^C &= I_{n-1}^2 \mu^2(\mathbf{W}^n) (2D_A^C + 2D_M^C \mu^2(\text{E}(\mathbf{y}_{n-1}))) \\ N_n^U &= I_{n-1} \eta(\mathbf{W}^n) (2D_A^U + 2D_M^U (1 + 2D_M^C) \eta(\text{E}(\mathbf{y}_{n-1}))) \\ N_n^{\text{prev}} &= I_{n-1}^2 \mu^2(\mathbf{W}^n) \left(1 + 2D_M^U \cdot \frac{\eta(\mathbf{W}^n)}{I_{n-1} \mu^2(\mathbf{W}^n)} \right) \times \\ &\quad (1 + 2D_M^C) \mu(\hat{\mathbf{F}}(\tilde{x}_{n-1}^t)). \end{aligned} \quad (6)$$

N_n^{prev} includes both, correlated and uncorrelated multiplicative noise, and operator $\hat{\mathbf{F}}$ as the influence of $f(\cdot)$. Equations (6) include square of mean values $\mu^2(\cdot)$ and the mean of square $\eta(\cdot)$ of coupling matrix \mathbf{W}^n , and depending on the particular type, noise propagation relies on $\mu^2(\cdot)$ and I_{n-1}^2 or $\eta(\cdot)$ and I_{n-1} as well as the input signal's mean. A DNN's topology therefore has a major influence on noise propagation due to its associated connection statistics.

II. NOISE IN SYMMETRIC DNNs

We initially focus on the influence of nonlinear function $f(\cdot)$, and hence start by considering a symmetric DNN where all connections $W_{ij}^n = 1/I_{n-1}$ are uniform.

As can be seen from Fig. 3(a-c), the SNR dependency for a DNN with our shifted sigmoid nonlinearity as activation function has two focusing points near $y = 0$ and $y = 1$. Orange data correspond to numerically obtained SNR values for a nonlinear DNN for the case of additive (a), multiplicative (b) and mixed (c) uncorrelated noise, and the SNR significantly differs to a single nonlinear neuron. Correlated noise leads to a similar SNR dependency, and only slight quantitative differences occur if the correlated noise intensity is of a similar amplitude as the uncorrelated noise (Fig. 3(d-f)). Only dispropor-

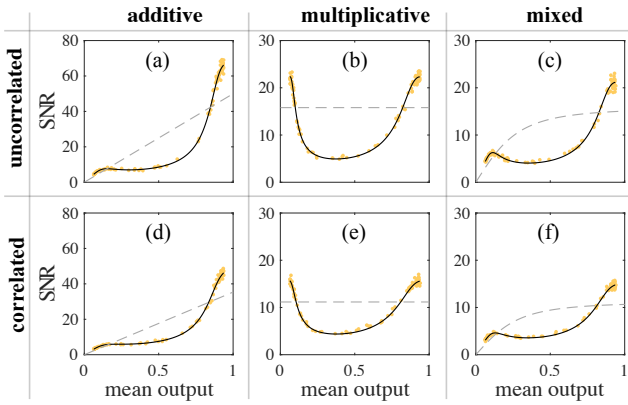


FIG. 3. Signal-to-noise ratio (SNR) of the output in a nonlinear DNN (orange). The analytical prediction is given by black solid line. Gray dashed line show the SNR for a linear FNN with the same noise parameters, which is identical to the SNR of a single nonlinear neuron. Top panels shows the impact of uncorrelated noise, and bottom panels correspond to correlated noise. Here we used $D_A^U = D_A^C = 10^{-4}$, $D_M^U = D_M^C = 10^{-3}$ and $\alpha = 4$.

tionally high noise intensities can lead to substantial qualitative modifications.

The SNR behaviour is determined by the general Eqs. (6), which can be simplified for symmetric DNNs. If the number of neurons in the previous layer I_{n-1} is large, the contribution of N_n^C dominates over N_n^U since $I_{n-1}^2 \mu^2(\mathbf{W}^n) = 1$ and $I_{n-1} \eta(\mathbf{W}^n) = 1/I_{n-1} \ll 1$. Noise originating from the previous layer N_n^{prev} has terms with both multipliers, and for symmetric DNN term $I_{n-1}^2 \mu^2(\mathbf{W}^n)$ dominates, hence $N_n^{\text{prev}} \approx (1 + 2D_M^C)\mu(\hat{\mathbf{F}}(\tilde{\mathbf{x}}_{n-1}^t))$. From this follows that N_n^U is much smaller than both N_n^C and N_n^{prev} in all hidden and the output layer

$$\text{Var}(\tilde{x}_{n,i}^t) \approx N_n^C + N_n^{\text{prev}}, \quad 2 < n \leq N. \quad (7)$$

The input layer has no previous layer, and therefore

$$\text{Var}(\tilde{x}_{n,i}^t) = N_n^C + N_n^U = \sigma_+^2 + \sigma_x^2(\mathbf{u}^t)^2, \quad n = 2. \quad (8)$$

A. First order approximation for nonlinear noise mixing

A first order approximation of nonlinear noise-mixing operator $\hat{\mathbf{F}}$ depends on the first derivative of activation function $f(\cdot)$, the expectation value and variance of $\tilde{x}_{n,i}^t$ as $\hat{\mathbf{F}}(\tilde{x}_{n,i}^t) \approx [f'(\mathbf{E}(\tilde{x}_{n,i}^t))]^2 \cdot \text{Var}(\tilde{x}_{n,i}^t)$ (see Ref.²⁴). If neurons are linear, as is the case for the input and output layers, this operator becomes $\hat{\mathbf{F}}(\tilde{x}_{n,i}^t) = \alpha^2 \text{Var}(\tilde{x}_{n,i}^t)$. Otherwise, in a DNN's nonlinear hidden layers $1 < n < N$, one obtains in first order

$$\begin{aligned} \hat{\mathbf{F}}(\tilde{x}_{n,i}^t) &\approx [f'(\mathbf{E}(\tilde{x}_{n,i}^t))]^2 \cdot \text{Var}(\tilde{x}_{n,i}^t) \\ &\approx [f'(\mathbf{E}(f^{-1}(y_{n,i}^t)))]^2 \cdot \text{Var}(\tilde{x}_{n,i}^t). \end{aligned} \quad (9)$$

As can be seen from Fig. 4(b), using a more nonlinear

The expectation value of $\tilde{x}_{n,i}^t$ was substituted by $f^{-1}(y_{n,i}^t)$ to maintain consistency with Eqs. 6.

With the above simplifications Eqs. (4–6) were used to predict the impact of noise for symmetric DNNs and demonstrate an excellent agreement with numerical simulation, see solid lines in Fig. 3. The final form of the set of equations for all layers with these simplifications is given in the Methods section.

For symmetric DNNs with uniform matrices $\hat{\mathbf{F}}(\tilde{x}_{n,i}^t) = \hat{\mathbf{F}}(\tilde{\mathbf{x}}_n^t)$, $\text{Var}(\tilde{x}_{n,i}^t) = \text{Var}(\tilde{\mathbf{x}}_n^t)$ due to averaging; $\mu(\cdot)$ in Eq. (6) can therefore be neglected. According to Eqs. (6,7) and (9), the variance of $\tilde{\mathbf{x}}_n^t$ can be rewritten in a closed recurrent form based on the same variable from the previous layer:

$$\begin{aligned} \text{Var}(\tilde{\mathbf{x}}_n^t) &= N_n^C + \\ (1 + 2D_M^C) &\left[f'(E(f^{-1}(\mathbf{y}_{n-1}^t))) \right]^2 \text{Var}(\tilde{\mathbf{x}}_{n-1}^t) \end{aligned} \quad (10)$$

with initial state $\text{Var}(\tilde{\mathbf{x}}_2^t) = \sigma_+^2 + \sigma_x^2(\mathbf{u}^t)^2$. Here, we consider the realistic case where all noise intensities are $\ll 1$, for which the contribution of N_n^C has only a minor impact. We can then neglect N_n^C , which allows us to focus on the consequence of network states propagating through a DNN's sequence of layers. Leveraging the symmetric topology we redefine $\text{Var}(\tilde{\mathbf{x}}_n^t) \approx S_n$ as a scalar sequence, and noise propagation of Eq. (10) transforms to a geometric progression

$$S_n = \left[f'(E(f^{-1}(\mathbf{y}_{n-1}^t))) \right]^2 \cdot S_{n-1}. \quad (11)$$

If $f'(\cdot) \leq 1$ on the entire interval of $y_n^t \in [0; 1]$, then sequence S_n decreases in general, otherwise it is increasing.

What this means in practice is that noise is kept from accumulating as long as the activation function's slope remains below unity. The here used activation functions and their first derivatives are shown in Fig. 4(a) for $\alpha = 2$ and 3, while Fig. 4(b) shows the variance inside a DNN until 12 layers for $\alpha = 2$ (top row) and $\alpha = 3$ (bottom row). Red lines correspond to analytical predictions based on Eq. (9), and points to numerical simulations. For our shifted sigmoid, the bifurcation in noise accumulation happens at $\alpha = 2$; for $\alpha \leq 2$ sequence S_n decreases and noise propagation through the DNN's layers is prevented. This is an extremely important insight. Firstly, it shows that under not too stringent conditions a DNN's SNR does not worsen when increasing its depth; for $\alpha = 2$ the variance remains essentially identical for all layers. Secondly, nonlinearity and a networks depth are in a general competition when an analogue DNN's SNR is crucial.

activation function with $\alpha = 3$ dramatically changes the

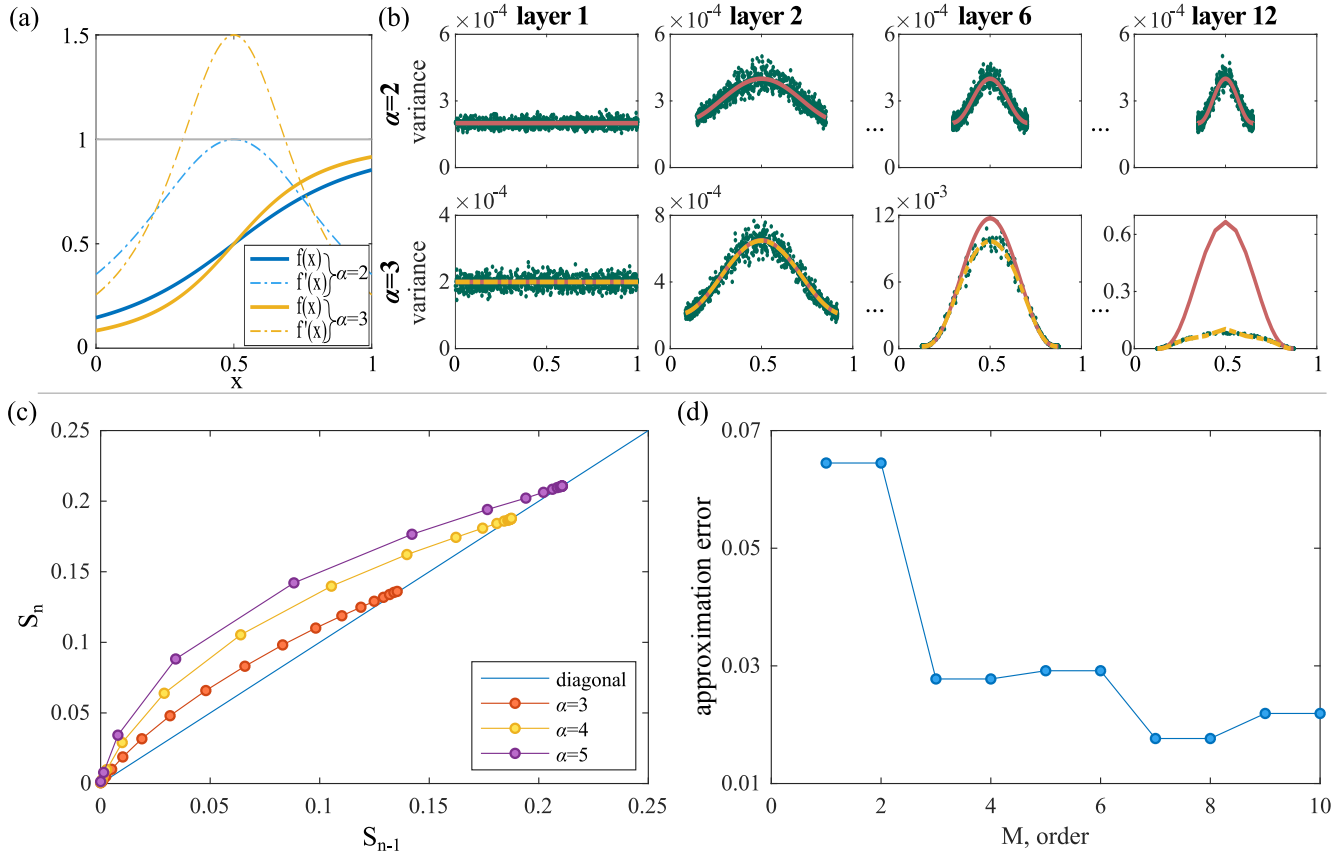


FIG. 4. (a) Activation functions and their first derivatives with $\alpha = 2$ (blue lines) and $\alpha = 3$ (orange lines). (b) Variance in different layers of a 12 layer DNN with $\alpha = 2$ (top row) and $\alpha = 3$ (bottom row). Red lines correspond to a first order approximation, yellow lines to a higher order approximation. (c) Lamerey diagram of S_n for three α values is shown in panel. (d) Approximation error depending on the Taylor series's order M . The noise is uncorrelated additive $D_A^U = 10^{-4}$.

situation: noise begins to accumulate and to strongly increase when adding hidden layers to the DNN. Furthermore, the now stronger nonlinearity results in a notable difference between the analytical description and numerical simulation, and this discrepancy increases as information propagates towards the deeper layers of the DNN. While the general behaviour of the variance curve is comparable to $\alpha = 2$, the variance's amplitudes start to strongly diverge.

We find that the speed at which variance $\text{Var}(\cdot)$ increases depends on the particular layer. Initially, growth is fast yet slows down for deeper layers and reaches a limit at some depth. This is well illustrated by a Lamerey diagram shown in Fig. 4(c), which demonstrates the numerically obtained evolution of S_n . As S_n approaches the diagonal $S_n = S_{n-1}$ growth slows down and noise amplitudes from one layer to the next remain constant, i.e. stop increasing. We evaluated several S_n with $\alpha > 2$, which all reached some limit, each at different depth and corresponding S_n limit. Two main rules emerged: the larger α , the larger the final S_n , yet also the fewer layers are required to reach the particular limit.

Though included, the data of S_n in Fig. 4(c) for $\alpha <$

2 is hardly visible. In this case the scale of S_n does not change with depth of the network, and S_n remains essentially constant at the single neuron level of 10^{-3} . All S_n values are therefore located near the origin of Fig. 4(c) for all $\alpha \leq 2$, and the SNR does not significantly surpass a single neuron's SNR for the generally valid assumption $I_n \gg 1$ for $n > 1$.

B. Higher order approximation

In order to explain the difference in Fig. 4(b) between our first order analytical approximation and numerical simulations, it is necessary to return to the reason why coefficient $f'(E(f^{-1}(y_{n-1}^t)))$ appeared in the first place. It determines the variance of nonlinear function $f(\cdot)$ for random variables. For a random variable X with mean value $\mu(X)$ and probability density distribution $p_X(x)$, $Y = f(X)$ has variance $\text{Var}(Y) = E(Y^2) - (E(Y))^2$ with $E(Y) = \int_{-\infty}^{\infty} f(x)p_X(x)dx$. Function $f(\cdot)$ can in general be approximated using a Taylor series of M th order. Equation (9), however, included only the Taylor series's 1st order, i.e. until the first derivative. After

several monotonous transformations, given in the Methods section, we arrive at the variance with M th order approximation

$$\begin{aligned} \hat{\mathbf{F}}(\tilde{\mathbf{x}}_n^t) \Big|_M &= \sum_{m=1}^M T_m^2 (V_{2m} - V_m^2) \\ &+ 2 \sum_{m=1}^M \sum_{i=1}^{m-1} T_m T_i (V_{m+i} - V_m V_i), \end{aligned} \quad (12)$$

or in a recurrent form based on the variance of the preceding order

$$\begin{aligned} \hat{\mathbf{F}}(\tilde{\mathbf{x}}_n^t) \Big|_M &= \hat{\mathbf{F}}(\tilde{\mathbf{x}}_n^t) \Big|_{M-1} + T_M^2 \cdot (V_{2M} - V_M^2) \\ &+ 2T_M \sum_{i=1}^{M-1} T_i (V_{M+i} - V_M V_i), \end{aligned} \quad (13)$$

where $T_m = \frac{1}{m!} f^{(m)}(\mu)(x - \mu)^m$ is the m th order term of the Taylor series approximated nonlinearity contribution and $V_m = \int_{-\infty}^{\infty} (x - \mu)^m p_X(x) dx$ is the m th moment of the probability density distribution $p_X(x)$.

Due to $S_n \approx \hat{\mathbf{F}}(\tilde{\mathbf{x}}_n^t)$, the higher order approximations of S_n strongly depend on probability density p_X and expectation value μ . These are known for the first two orders: V_1 is equal to zero and $V_2 = \text{Var}(\tilde{\mathbf{x}}_n^t)$. The preceding terms need to be specifically calculated.

Figure 4(b) shows S_n obtained via the approximation of $\hat{\mathbf{F}}$ until the 15th order as yellow lines. Figure 4(d) shows the discrepancy between our analytical approximation based on different orders and the full-nonlinearity based numerical solutions at the point of the largest variance, found at output $\tilde{x} = 0.5$, which is also where the largest discrepancy between analytic and numerical solutions are found. Interestingly, differences between analytical approximation and numerical calculations are arranged in pairs: every second point provides the same accuracy as an approximation based on its preceding order. This is because every even derivative of $f(\cdot)$ is zero at the point of inflection at $\tilde{x} = 0.5$, and the higher order approximation following an uneven order M therefore has the same value.

In general, for $M \rightarrow \infty$ a Taylor series approximates a function on the whole set of values, not only in a small neighbourhood. However, in our setting only interval $[0; 1]$ is of relevance, and for some M a better global approximation simultaneously approximates with less accuracy inside $[0, 1]$. For this reason, Fig. 4(d) shows a globally decreasing sequence, but some higher orders might result in a worse approximation than their preceding orders.

III. NOISE IN FULLY TRAINED DNNs

Training DNNs is based on changing connection matrices and biases, and naturally weight matrices and their statistical properties differ depending on tasks and training methods. Crucially, due to the typically large number

of neurons in hidden layers, weight as well as bias distribution statistics after training are sufficient to describe noise propagation in trained nonlinear DNNs.

We therefore consider a coupling matrix as a set of random variables, whose statistical properties such as mean square and squared mean are essential for variance calculations. The analysis for uniform networks given in Sect. II remains mostly valid for trained networks, except for an admittedly cumbersome modification to S_n

$$\begin{aligned} S_n &\approx I_{n-1}^2 \mu^2(\mathbf{W}^n) \cdot [2D_A^C + 2D_M^C \mu^2\{\mathbf{E}(\mathbf{y}_{n-1}^t)\}] + \\ &I_{n-1} \eta(\mathbf{W}^n) \cdot [2D_A^U + 2D_M^U (1 + 2D_M^C) \cdot \eta(\mathbf{E}(\mathbf{y}_{n-1}^t))] \\ &+ I_{n-1} \eta(\mathbf{W}^n) (1 + \sigma_X^2) \cdot \eta\{f'(f^{-1}(\mathbf{E}(\mathbf{y}_{n-1}^t)))\} S_{n-1}, \end{aligned} \quad (14)$$

with initial value $S_2 = \sigma_+^2 + \sigma_X^2 \mu^2(\mathbf{u}^t)$ as for symmetric DNNs. After training a DNN model, the squared mean $\mu^2(\mathbf{W}^n)$ and mean square $\eta(\mathbf{W}^n)$ of connection matrices remain static and are known, yet $\mathbf{E}(\mathbf{y}_{n-1}^t)$ and $f'(f^{-1}(\mathbf{E}(\mathbf{y}_{n-1}^t)))$ needs to be approximated as it depends on the particular input information. The relevant SNR-contributions related to the expectation values of neurons then are

$$\begin{aligned} \mu(\mathbf{E}(\mathbf{y}_n)) &= \int_{-\infty}^{\infty} f(z) p_n^*(z) dz \\ \eta(\mathbf{E}(\mathbf{y}_n)) &= \int_{-\infty}^{\infty} (f(z))^2 p_n^*(z) dz \\ \eta(f'(f^{-1}(\mathbf{E}(\mathbf{y}_n)))) &= \int_{-\infty}^{\infty} (f'(z))^2 p_n^*(z) dz, \end{aligned} \quad (15)$$

where $p_n^*(z)$ is the probability density of neuron states $\tilde{\mathbf{x}}_n$ under the influence of the activation function $f(\cdot)$. When investigating different computational tasks we found that distribution $p_n^*(\cdot)$ can be well approximated only utilizing the weights' statistics after training and the input data. Details are given in Methods VI B.

In order to demonstrate the validity of our approach approach works for DNNs regardless of the specific task, we trained three noiseless networks for different tasks: DNN A - classification of handwritten digits (MNIST digits); DNN B - classifying clothing images (MNIST fashion); DNN C - analogue target approximation while predicting a chaotic Mackey-Glass sequence²⁵. Furthermore, DNN A is trained and tested using a constant, hence not optimized bias for each neuron, while network B has optimized biases in each layer. The resulting statistics of biases and coupling matrices are given in Appendix A. Connection weights and biases are optimized during training based on an Adam optimization algorithm, and their values can be positive and negative. All three networks were trained using the Keras neural-network library²⁶. To build our network we have used brain.js²⁷.

Deep neural networks have demonstrated excellent performance for image classification²⁸. To enable comparison with the previous sections, we continue using two hidden layers with 200 neurons. Crucially, the analytical approximation can readily be extended to other topologies, i.e. deeper networks with larger layers or DNNs

with a convolutional topology. Here we use a sigmoid without shift $f(\tilde{x}) = 1/(1 + e^{-\tilde{x}})$ as activation function. For training and testing handwritten digit recognition we used the MNIST database containing more than 10000 images. Each image consists of 28×28 pixels in a gray scale, resulting in 784 input nodes. For classifying digits 0–9 the system has 10 output neurons, and the result is determined by the output neuron with the largest value. The trained DNN A has an averaged training error of $\approx 1\%$ and testing error of $\approx 1\%$ averaged across all digits.

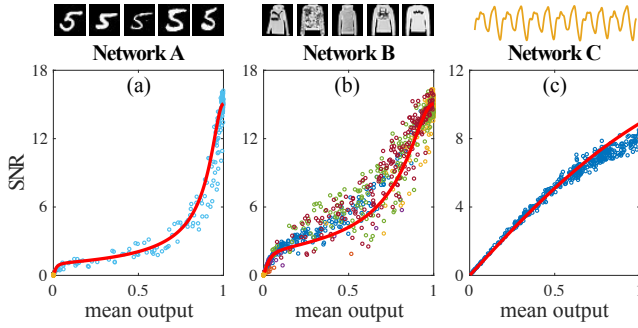


FIG. 5. SNR for the output layers of three networks: A – digits recognition (a) tested on 1000 images of digit “5”; B – clothing detection (b) tested on 1000 images of “pullovers”; C – prediction of Mackey–Glass system realization . The solid lines correspond to analytical prediction. The analytic approximation depends on approximation $p^*(z)$

The SNR dependency is numerically obtained as before using the trained network topologies, yet now under noisy conditions. Each input image is repeated K times to calculate the expected value and the standard deviation. Figure 5(a) shows the SNR in the final layer for different example images of digit “5” as input, which is comparable to the SNR for all 10 different digits. Blue data in Fig. 5(a) corresponds to the class of digit “5”, and data is distributed across the entire range. Yellow data corresponds to the remaining 9 other classes, and a strong focus to small mean amplitudes illustrates successful classification. The red solid line is our analytical prediction based on a first order approximation, which is in very good agreement with numerical simulations.

The similar network but now also optimizing biases during training is considered for the MNIST-fashion data set. This data set contains images of clothes and shoes with T-shirt/top, Trouser, Pullover, Dress, Coat, Sandal, Shirt, Sneaker, Bag, Ankle boot as labels. Again, input data is a 28×28 pixel image. Figure 5(b) shows the output layer SNR for 1000 images of pullovers. The analytically predicted dependency (solid line) works well in this case too. In this task DNN B obtained a 5% training and 10% testing error rate,

Feed forward networks usually are used for classification tasks. In order to emphasize the generality of our analytical framework, we consider the following example for analogue signal prediction. The DNN’s input nodes

receive the 100 previous points of a chaotic Mackey–Glass system²⁹ at each time t . The network’s output is then tasked to predict the next point of the chaotic sequence. The network therefore has 100 input neurons and one output neuron, and the hidden layers contain 200 neurons, as previously. After training using Keras the network achieves 87% precision. Figure 5(c) shows the SNR in the output layer, and the red solid lines show the predicted dependency, which is in good agreement with our numerical simulation.

IV. DISCUSSION AND CONCLUSION

In this article we studied the effect of internal noise on the output of DNNs. Several models of different complexity were considered. The general features depending on the DNN’s nonlinear activation function and depth were shown for the symmetric DNNs with full and uniform connectivity. The SNR depends on both the nonlinear function and the type of noise involved. The analytical methods approximate the noise level in all layers very well.

All obtained results were validated for three trained DNNs used for digits recognition, clothing detection and time series prediction, and an excellent agreement of the obtained results with the prediction was obtained regardless of DNN topology. Crucially, our analytical approximations only depend on connection and bias statistics. Our method therefore is agnostic to the detailed, local configuration of neurons and connections. This is crucial when it comes to approximating the SNR performance of a real, hardware implemented DNN. One can employ a numerical toy-model with the general parameters of the hardware system such as activation functions and their noise amplitudes and characteristics, which usually are readily available. The toy model is then trained, and while the local configuration of a hardware DNN will not correspond to the trained toy model^{23,30}, bias and connection statistics are likely to be similar.

A very interesting and highly relevant result is the SNR’s behaviour when the network depth is increased. We initially (and quite intuitively) expected to find the noise level to continue increasing as a function of the number of layers. However, we demonstrated that the output layer’s SNR is generally bound by a lower limit. A DNN’s SNR does therefore not worsen when layers are added once this limit is reached, and the exact value is determined mainly by the activation function’s degree of nonlinearity. Most importantly, we find (i) that nonlinearity and weight statistics efficiently avoid accumulation of correlated noise, and (ii) that propagation and accumulation of noise from one to the next layer is fully suppressed when using activation functions with a slope smaller than unity. These are very easy and realistically satisfiable requirements, and the output SNR for such hardware DNNs is essentially identical to the one of a single neuron. It therefore should be plausible and realistic to

design and implement analog hardware DNNs which are very robust to internal noise.

Future work needs to consider more specific network topologies and to elaborate if our general and promising findings can be confirmed for potentially more restricted connection matrices. Further efforts should focus on deriving the accumulative SNR for a particular task, hence to obtain to obtain an upper accuracy limit imposed by the DNN's internal noise. Finally, our work provides important insight towards DNN topologies with enhanced noise resilience. The identification of architectures that provide noise robustness and concepts that leverage potential benefits of noise on learning learning³¹ is an important future line of research. This also raises the question which role nonlinear and hierarchical structure play in biological NNs.

V. ACKNOWLEDGMENTS

The authors acknowledge the support of the Region Bourgogne- Franche-Comté. This work was supported by the EUR EIPHI program (Contract No. ANR-17-EURE-0002) and the Volkswagen Foundation (NeuroQNet II). N.S. is supported by the Vernadski scholarship of the French Government.

VI. METHODS

A. Noise propagation in symmetric FNNs

The output of a single neuron is described by Eq. (3). The expectation value of the output from the i th neuron of the n th layer is

$$\mathbb{E}[y_{n,i}^t] = \mathbb{E}[x_{n,i}^t]. \quad (16)$$

According to general rules of mathematical operations for uncorrelated random variables X and Y , one obtains $\text{Var}[X + Y] = \text{Var}[X] + \text{Var}[Y]$ and $\text{Var}[X \cdot Y] = \text{Var}[X] \cdot (\mathbb{E}[Y])^2 + ((\mathbb{E}[X])^2 + \text{Var}[X]) \cdot \text{Var}[Y]$. When X is multiplied on a constant C , the variance becomes $\text{Var}[C \cdot X] = C^2 \text{Var}[X]$. All considered noise sources ξ have zero expected value and a variance equal to 1. The final variance of the noise source is controlled by the corresponding noise intensity, and $\text{Var}(\sqrt{2D_A^U \xi_{n,i}^{U,A}}) = 2D_A^U$. Taking the above into account, the variance of $y_{n,i}^t$ can be calculated as:

$$\begin{aligned} \text{Var}[y_{n,i}^t] &= 2D_A^U + 2D_A^C + \\ \text{Var}[x_{n,i}^t(1 + \sqrt{2D_M^C \xi_n^{C,M}})(1 + \sqrt{2D_M^U \xi_{n,i}^{U,M}})] &= 2D_A^U + 2D_A^C + 2D_M^U (\mathbb{E}[x_{n,i}^t])^2 + \\ (1 + 2D_M^U) \text{Var}[x_{n,i}^t(1 + \sqrt{2D_M^C \xi_{n,i}^{C,M}})] &= 2D_A^U + 2D_A^C + (2D_M^U + 2D_M^C + 4D_M^U D_M^C) \times \\ (\mathbb{E}[x_{n,i}^t])^2 + (1 + 2D_M^U)(1 + 2D_M^C) \text{Var}[x_{n,i}^t]. \end{aligned} \quad (17)$$

According to σ_+^2 and σ_x^2 introduced in Sect. IB, Eq. (1) can be simply rewritten in the form of Eq. (5).

The variance of the combined signal, propagating from layer n to layer $(n+1)$, $\tilde{x}_{n+1,i}^t$ is

$$\begin{aligned} \text{Var}[\tilde{x}_{n+1,i}^t] &= \text{Var}\left[\sum_{j=1}^{I_n} W_{ij}^{n+1} y_{n,j}^t + b_{n+1,i}\right] = \\ \text{Var}\left[\sum_{j=1}^{I_n} W_{ij}^{n+1} y_{n,j}^t\right]. \end{aligned} \quad (18)$$

Some terms of $y_{n,j}^t$ are independent of index j , and they therefore can be moved outside the sum. Moreover, almost all variables in Eq. (18) depend on time. We can therefore neglect index t and include it only in the final equations.

$$\begin{aligned} \text{Var}[\tilde{x}_{n+1,i}] &= \text{Var}\left[(1 + \sqrt{2D_M^C} \xi_n^{C,M}) \times \right. \\ &\quad \left. \sum_{j=1}^{I_n} W_{ij}^{n+1} (1 + \sqrt{2D_M^U} \xi_{n,j}^{U,M}) x_{n,j} + \right. \\ &\quad \left. \sqrt{2D_A^U} \sum_{j=1}^{I_n} W_{ij}^{n+1} \xi_{n,j}^{U,A} + \sqrt{2D_A^C} \xi_n^{C,A} \sum_{j=1}^{I_n} W_{ij}^{n+1}\right] \\ &= 2D_A^U \sum_{j=1}^{I_n} (W_{ij}^{n+1})^2 + 2D_A^C \left(\sum_{j=1}^{I_n} W_{ij}^{n+1}\right)^2 + \\ &\quad 2D_M^C \left(\mathbb{E}\left[\sum_{j=1}^{I_n} W_{ij}^{n+1} x_{n,j}\right]\right)^2 + (1 + 2D_M^C) \times \\ &\quad \text{Var}\left[\sum_{j=1}^{I_n} W_{ij}^{n+1} (1 + \sqrt{2D_M^U} \xi_{n,j}^{U,M}) x_{n,j}\right] \end{aligned} \quad (19)$$

The connection matrix \mathbf{W}^{n+1} has the mean of square value $\eta(\mathbf{W}^{n+1}) = \frac{1}{I_n I_{n+1}} \sum_{i=1}^{I_{n+1}} \sum_{j=1}^{I_n} (W_{ij}^{n+1})^2$ and mean value $\mu(\mathbf{W}^{n+1}) = \frac{1}{I_n I_{n+1}} \sum_{i=1}^{I_n} \sum_{j=1}^{I_{n+1}} W_{ij}^{n+1}$. The square of the last we denote as $\mu^2(\cdot)$. Vector \mathbf{x}_n has some averaged expected value $\mu(\mathbb{E}[\mathbf{x}_n])$ and mean variance $\mu(\text{Var}[\mathbf{x}_n])$. Again, both can be moved outside the sum, and therefore

$$\begin{aligned} \text{Var}(\tilde{x}_{n+1,i}^t) &\approx 2D_M^C I_n^2 \mu^2(\mathbf{W}^{n+1}) \mu^2(\mathbb{E}[\mathbf{x}_n]) + \\ 2D_A^U I_n \eta(\mathbf{W}^{n+1}) + 2D_A^C I_n^2 \mu^2(\mathbf{W}^{n+1}) + & \\ (1 + 2D_M^C) \mu^2(\mathbb{E}[\mathbf{x}_n]) \times \text{Var}\left[\sum_{j=1}^{I_n} W_{ij}^{n+1} \times \right. & \\ \left. (1 + \sqrt{2D_M^U} \xi_{n,j}^{U,M})\right] + \mu(\text{Var}[\mathbf{x}_n]) (1 + 2D_M^C) \times & \\ \left(\left(\sum_{j=1}^{I_n} W_{ij}^{n+1}\right)^2 + \sum_{j=1}^{I_n} 2D_M^U (W_{ij}^{n+1})^2\right) = & \\ I_n^2 \mu^2(\mathbf{W}^{n+1}) \cdot (2D_A^C + 2D_M^C (\mu(\mathbb{E}[\mathbf{x}_n]))^2) + & \\ I_n \eta(\mathbf{W}^{n+1}) \cdot (2D_M^U (1 + 2D_M^C) (\mu(\mathbb{E}[\mathbf{x}_n]))^2 + & \\ 2D_A^U) + I_n^2 \mu^2(\mathbf{W}^{n+1}) \left(1 + \frac{\eta(\mathbf{W}^{n+1})}{I_n \mu(\mathbf{W}^{n+1})} 2D_M^U\right) \times & \\ (1 + 2D_M^C) \mu(\text{Var}[\mathbf{x}_n]). \end{aligned} \quad (20)$$

In the case of symmetric DNNs, $I_n^2 \mu(\mathbf{W}^{n+1}) = 1$ and $I_n \eta(\mathbf{W}^{n+1}) = 1/I_n$. When $I_n \gg 1$, all terms with $I_n \eta(\mathbf{W}^{n+1})$ can be neglected.

$$\text{Var}[\tilde{x}_{n+1,i}^t] \approx 2D_A^C + 2D_M^C \mu^2(\mathbb{E}[\mathbf{x}_n]) + (1 + 2D_M^C) \mu(\text{Var}[\mathbf{x}_n]). \quad (21)$$

If $I_n = 1$, as in the first layer, then $I_n^2 \mu(\mathbf{W}^{n+1}) = I_n \eta(\mathbf{W}^{n+1})$ and the variance this layer becomes

$$\text{Var}[\tilde{x}_{n+1,i}^t] = \sigma_+^2 + \sigma_x^2 (E[x_n^t])^2 + (1 + \sigma_x^2) \mu(\text{Var}[x_n^t]). \quad (22)$$

Thus, the general equations of variance in symmetric DNNs are

$$\begin{aligned} \text{Var}[\tilde{x}_1^t] &= \text{Var}[x_1^t] = 0 \\ \text{Var}[\tilde{x}_{2,i}^t] &= \sigma_+^2 + \sigma_x^2 (E[x_1^t])^2. \end{aligned} \quad (23)$$

The corresponding variance in hidden and output layers is described by Eq. (21). The final output variance from any layer can be calculated using Eq. (5).

Higher order approximation of operator \hat{F} .

Operator \hat{F} , introduced in Sect. II B, describes the variance of some random variable Y which is equal to nonlinear function of another random variable: $Y = f(X)$. In general, variance is the difference between the expectation value of a squared variable and the square of expectation value. In order to calculate expectation values, nonlinear function $f(\cdot)$ has to be approximated, for which we use its Taylor series

$$\begin{aligned} f(x) &\approx \sum_{m=0}^M \frac{1}{m!} f^{(m)}(\mu) (x - \mu)^m \approx \\ \sum_{m=0}^M T_m (x - \mu)^m &\approx f(\mu) + \sum_{m=1}^M T_m (x - \mu)^m, \end{aligned} \quad (24)$$

where $f^{(m)}$ denotes the m th derivative of function $f(\cdot)$, $T_m = \frac{1}{m!} f^{(m)}(\mu)$. If variable X has the probability density distribution $p_X(x)$, then the expected value of Y is

$$\begin{aligned} E[Y] &= \int_{-\infty}^{+\infty} f(x) p_X(x) dx \approx \int_{-\infty}^{+\infty} f(\mu) p_X(x) dx + \\ &\quad \int_{-\infty}^{+\infty} \left(\sum_{m=1}^M T_m (x - \mu)^m \right) p_X(x) dx = \\ &\quad f(\mu) + \sum_{m=1}^M T_m V_m, \end{aligned} \quad (25)$$

where $V_m = \int_{-\infty}^{+\infty} (x - \mu)^m p_X(x) dx$. The expected value of the square can be calculated in a similar way:

$$\begin{aligned} E[Y^2] &\approx \int_{-\infty}^{+\infty} \left(f(\mu) + \sum_{m=1}^M T_m V_m \right)^2 p_X(x) dx = \\ &\quad (f(\mu))^2 + 2f(\mu) \sum_{m=1}^M T_m V_m + \sum_{m=1}^M T_m^2 V_{2m} + \\ &\quad 2 \sum_{m=1}^M \sum_{i=1}^{m-1} T_m T_i V_{m+i}. \end{aligned} \quad (26)$$

Using the square of Eqs. (25,26), the variance of the M th order is

$$\begin{aligned} \text{Var}[Y] \Big|_M &= E[Y^2] - (E[Y])^2 = \sum_{m=1}^M T_m^2 V_{2m} + \\ &\quad 2 \sum_{m=1}^M \sum_{i=1}^{m-1} T_m T_i V_{m+i} - \left(\sum_{m=1}^M T_m V_m \right)^2, \end{aligned} \quad (27)$$

which can simply be rearranged into Eq. (12). For some cases it would be more convenient to use the recurrent equation based on the approximation of the previous order:

$$\begin{aligned} \text{Var}[Y] \Big|_M &= 2 \sum_{m=1}^{M-1} \sum_{i=1}^{m-1} T_m T_i V_{m+i} + T_M^2 V_{2M} + \\ &\quad \sum_{m=1}^{M-1} T_m^2 V_{2m} - \left(\sum_{m=1}^{M-1} T_m V_m \right)^2 - \left(\sum_{m=1}^{M-1} T_m V_m \right)^2 - \\ &\quad T_M^2 V_M^2 = \text{Var}[Y] \Big|_{M-1} + T_M^2 (V_{2M} - V_M^2) - \\ &\quad 2 T_M \sum_{i=1}^{M-1} T_i (V_{M+i} - V_M V_i), \end{aligned} \quad (28)$$

which again can be rearranged into Eq. (13).

As an example, let us consider the cubic nonlinear function $f(x) = 3x^2 - 2x^3$, which reassembles a sigmoid function in the range $(0; 1)$. This nonlinearity has no parameters, and its second derivative is always larger one near $x = 0.5$. The first order approximation based on Eq. (9) therefore leads to a growing error for deep networks, as was observed in Sect. II for sigmoid function with $\alpha > 2$.

The new nonlinearity is cubic, so the maximal order of Taylor series approximation to precisely reproduce this function is $M = 3$. The Taylor series terms are $T_1 = 6(\mu - \mu^2)$, $T_2 = 3(1 - 2\mu)$, $T_3 = -2$, and when $\mu = 0.5$ they transform to $T_1 = 1.5$, $T_2 = 0$, $T_3 = -2$. Calculating the required V -values is less straight forward. For any random X it always holds that $V_1 = 0$ and $V_2 = \text{Var}[X]$. The following terms strongly depend on the probability distribution of X , and can be calculated only if $p_X(x)$ is known or can be well approximated. For example, if X has a normal distribution, then $V_3 = V_5 = 0$, $V_4 = 3(\text{Var}[X])^2$, $V_6 = 15(\text{Var}[X])^3$.

B. Approximation of state probability $p^*(\cdot)$

In order to approximate the impact of noise in trained DNNs we need to take the influence of bias and connection matrices into account, which were introduced in Eq. (15). The probability density distribution $p_n^*(z)$ of \tilde{x}_n takes part in all terms of Eq. (15).

One can make the weak assumption that, for DNN's with many neurons in its hidden layers, $p_n^*(z)$ to be some well behaved function, such as uniform or normal distributions. Figure 6(a-c) shows the SNR for DNN A, based on weight statistics using uniform (red line) and normal (green line) distributions.

Reaching a quantitative agreement based on the statistics of weights requires approximating function $p_n^*(z)$. Here, we use $g(x) = \exp(c_4 x^4 + c_3 x^3 + c_2 x^2 + c_1 x + c_0)$ for our approximation. It allows approximating bimodal, normal and uniform distributions and hence captures a wide range of cases which excellently approximate all conditions we observed for DNNs trained for classifying as well as for continuous function approximation. The

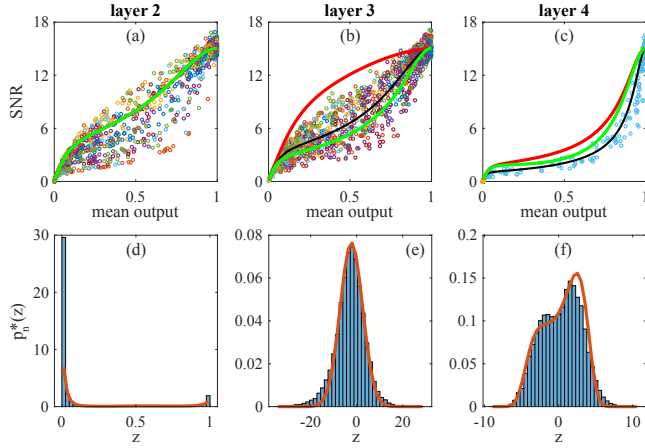


FIG. 6. SNR in hidden and output layers of Network A, used for digits recognition are given in panels (a,b,c). Red, green and black lines correspond to analytical prediction based on assumption of uniform, normal and using $g(\tilde{x})$ for approximating $p_n^*(z)$, respectively. The probability distribution of \tilde{x}_n in layers 2,3,4 and corresponding approximating curves are shown in panels (d-f).

analytical prediction of SNR curve based on this approximation is given in Fig. 6(a–c) by black line. As can be seen from Fig. 6(d–f) the obtained analytical prediction is in a good agreement with the statistics of \tilde{x}_n in each layer.

Analytics based on the approximated $p_n^*(z)$ via $g(\tilde{x})$ demonstrated the best agreement with numerical simulation. At the same time, uniform and normal distributions do to some degree produce similar behaviour. They do not demonstrate such good quantitative agreement.

- ¹J. Hasler and B. Marr, *Frontiers in neuroscience* **7**, 118 (2013).
- ²D. Brunner, M. C. Soriano, C. R. Mirasso, and I. Fischer, *Nature communications* **4**, 1364 (2013).
- ³T. Tuma, A. Pantazi, M. Le Gallo, A. Sebastian, and E. Eleftheriou, *Nature Nanotechnology* **11**, 693 (2016).
- ⁴Nature **547**, 428 (2017).
- ⁵D. Psaltis, D. Brady, X.-G. Gu, and S. Lin, *Nature* **343**, 325 (1990).
- ⁶J. Bueno, S. Maktoobi, L. Froehly, I. Fischer, M. Jacquot, L. Larger, and D. Brunner, *Optica* **5**, 756 (2018).
- ⁷X. Lin, Y. Rivenson, N. T. Yardimci, M. Veli, M. Jarrahi, and A. Ozcan, *Science* **26**, 1 (2018).
- ⁸Y. Shen, N. C. Harris, S. Skirlo, M. Prabhu, T. Baehr-Jones,

- M. Hochberg, X. Sun, S. Zhao, H. Larochelle, D. Englund, and M. Soljacic, *Nature Photonics* **11**, 441 (2017).
- ⁹A. N. Tait, T. F. De Lima, E. Zhou, A. X. Wu, M. A. Nahmias, B. J. Shastri, and P. R. Prucnal, *Scientific Reports* **7**, 1 (2017).
- ¹⁰J. Moughames, X. Porte, M. Thiel, G. Ulliac, L. Larger, M. Jacquot, M. Kadic, and D. Brunner, *Optica* **7**, 640 (2020).
- ¹¹Dinc, Niyazi Ulas, Psaltis, Demetri, and Brunner, Daniel, *Photoniques* , 34 (2020).
- ¹²J. Moughames, X. Porte, L. Larger, M. Jacquot, M. Kadic, and D. Brunner, *Opt. Mater. Express* **10**, 2952 (2020).
- ¹³S. Gupta, A. Agrawal, K. Gopalakrishnan, and P. Narayanan, *Proceedings of the 32nd International Conference on International Conference on Machine Learning* **37**, 1737 (2015).
- ¹⁴M. C. Soriano, S. Ortín, D. Brunner, L. Larger, C. R. Mirasso, I. Fischer, and L. Pesquera, *Opt. Express* **21**, 12 (2013).
- ¹⁵N. Semenova, X. Porte, L. Andreoli, M. Jacquot, L. Larger, and D. Brunner, *Chaos: An Interdisciplinary Journal of Nonlinear Science* **29**, 103128 (2019), <https://doi.org/10.1063/1.5120824>.
- ¹⁶J. Feldmann, N. Youngblood, M. Karpov, H. Gehring, X. Li, M. Stappers, M. Le Gallo, X. Fu, A. Lukashchuk, A. S. Raja, J. Liu, C. D. Wright, A. Sebastian, T. J. Kippenberg, W. H. P. Pernice, and H. Bhaskaran, *Nature* **589**, 52 (2021).
- ¹⁷S. Moon, K. Shin, and D. Jeon, *IEEE Transactions on Very Large Scale Integration (VLSI) Systems* **27**, 1455–1459 (2019).
- ¹⁸D. Janke and D. V. Anderson, in *2020 IEEE 63rd International Midwest Symposium on Circuits and Systems (MWSCAS)* (2020) pp. 150–153.
- ¹⁹B. Dolenko and H. Card, *Electronics letters* **29**, 693 (1993).
- ²⁰J. Misra and I. Saha, *Neurocomputing* **74**, 239 (2010), *artificial Brains*.
- ²¹A. A. Dibazar, A. Bangalore, Hyungook Park, S. George, W. Yamada, and T. W. Berger, in *The 2006 IEEE International Joint Conference on Neural Network Proceedings* (2006) pp. 2015–2022.
- ²²M. C. Soriano, S. Ortín, L. Keuninckx, L. Appeltant, J. Danckaert, L. Pesquera, and G. van der Sande, *IEEE transactions on neural networks and learning systems* **26**, 388–393 (2015).
- ²³L. Andreoli, X. Porte, S. Chrétien, M. Jacquot, L. Larger, and D. Brunner, *Nanophotonics* **9**, 4139 (2020).
- ²⁴J. R. Benjamin and C. A. Cornell, *Probability, Statistics, and Decision for Civil Engineers* (Dover Publications, 2014).
- ²⁵H. Jaeger and H. Haas, *Science* **304**, 78 (2004), <https://science.sciencemag.org/content/304/5667/78.full.pdf>.
- ²⁶F. Chollet *et al.*, GitHub (2015), <https://github.com/fchollet/keras>.
- ²⁷“brain.js,” <https://github.com/BrainJS> (2021).
- ²⁸Y. LeCun, <http://yann.lecun.com/exdb/mnist/index.html> (2021).
- ²⁹M. Mackey and L. Glass, *Science* **197**, 287 (1977), <https://science.sciencemag.org/content/197/4300/287.full.pdf>.
- ³⁰M. Freiberger, P. Bienstman, and J. Dambre, *Scientific Reports* **10**, 14451 (2020).
- ³¹A. Murray, *Electronics Letters* **27**, 1546 (1991).